ISBN: 978-3-95450-184-7 doi:10.18429/JACoW-IPAC2018-TUPAK013

GEANT4 SIMULATION OF RADIATION EFFECT ON THE DEFLECTOR OF EXTRACTION SYSTEM IN HUST SCC250

S. W. Hu, L. G. Zhang, Z. Y. Mei, Z. J. Zeng, X. F. Li, K. J. Fan†
Institute of Applied Electromagnetic Engineering, Huazhong University of Science and Technology, Wuhan, China

Abstract

China has payed extensive attention to the development of proton therapy in recent years. When design a compact, high energy superconducting cyclotron for proton therapy, radiation effect induced by beam losses is a crucial consideration. Since the proton beam is extracted out of HUST SCC250 by electrostatic deflectors, the fierce interaction between proton beam and the deflector septum is the main cause of beam losses, which will bring about radiation effect leading to activation and coil quench. This paper presents simulation results of radiation effect by utilizing Geant4 Monte Carlo code. The energy depositions of proton beam in various septum materials are compared. Meanwhile, the yields, the energy and angular distributions of secondary particles are investigated. Those simulation results based on radiation effect will provide us with valuable implications for the design of this superconducting cyclotron.

INTRODUCTION

HUST SCC250, being developed for/at Huazhong University of Science and Technology, is a superconducting cyclotron applied for proton therapy. The 250MeV proton beam is extracted at nearly 0.8m radius and the beam current is about 800nA. The electrostatic deflector in this cyclotron is the research subject of this paper, of which structure has been introduced in another paper [1]. In practical operating conditions, the deflector undergoes intense interactions with beam that will directly influence the beam quality and extraction efficiency. These interactions subsequently cause severe cooling issue and radiation effect affecting the operating performance of the cyclotron. The cooling problem has been discussed in another paper [1], and the radiation effect is studied in this paper.

Radiation effect exerts considerable influences on the operation of superconducting cyclotron from the following two main aspects: the nuclear heating of the superconducting magnet and radiation damage or activation of certain materials [2]. The nuclear heating happens when the primary and secondary particles deposit their energy into the magnet leading to temperature rise, so that the cryogenic magnet is faced with high risk of quench. Radiation damage occurs on the insulators or superconducting windings showing poor working performances when they are exposed to high radiation fluences. To give a detailed description of radiation effect, Geant4 toolkit has been used to model the interactions between septum and proton beam. That the energy depositions and generated secondary particles have been analysed gives a valuable reference to the future study and configuration of the cyclotron.

MATERIAL AND MEHTODS

Incident Beam Properties

As the proton beam is propagated along the +Z axis into the deflector, its transverse motion can be represented by two ellipses in the phase spaces [3] (X, X_P) and (Y, Y_P), where $X_P = P_x/P_z$, $Y_P = P_y/P_z$, represent the beam angular divergences θ and φ respectively, and P_x, P_y, P_z stand for the three components of the beam momentum. The phase ellipse is defined with Twiss parameters and beam emittance. The beam emittance is 3mm·mrad. Twiss parameters taken from beam dynamics calculation are tabulated in Table 1.

Table 1: Twiss Parameters of Incident Beam

X plane	Y plane
$\alpha_x = -0.534$	$\alpha_y = 0.220$
$\beta_x = 1.304$	$\beta_y = 0.668$
$\gamma_x = 0.986$	$\gamma_y = -1.569$

It is worth mentioning that Geant4 code package offers PrimaryGenarationAction.cc class to determine the incident beam properties. Geant4 code provides SetParticleMomentumDirection( ) function for users to set the momentum direction of particles. The proton beam energy in our study is set to be monoenergetic 250MeV.

Geant4 10.1.2 edition is employed in this study and the application platform is Win10 x64 system.

Simulation Set-ups

Since most of the beam losses occur at the entrance edge of the deflector, to simplify the calculation, we establish 1/4 length of the overall deflector to be simulation model whose outline 3D dimension is 40mm×50mm×120mm. As shown in Fig. 1, a spherical scoring detector surrounding the deflector (radius = 100mm, thickness = 1mm) is implemented. To count the secondary particle fluences in the outer space, the scoring geometry is divided into 36 angular bins (10°each) originated from the +X axis. The septum is only 0.3mm thick, of which material is chosen from tungsten(W), tantalum(Ta) and molybdenum(Mo), since those three alternatives are most likely to be used in the deflector. The whole model is placed in 2×10^{-5}Pa vacuum environment.

† kjfan@hust.edu.cn

ISBN: 978-3-95450-184-7 doi:10.18429/JACoW-IPAC2018-TUPAK013

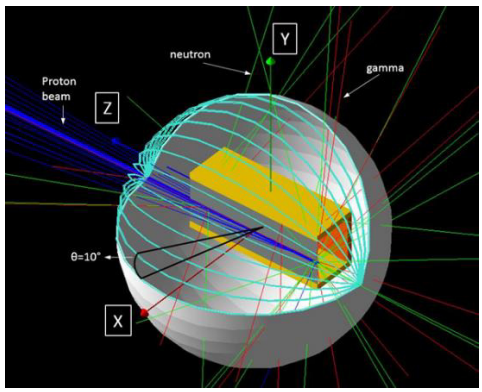

Figure 1: Simulation model in Geant4.

Note that the selection of physics model is of great significance when utilizing Geant4 to simulate the interactions between particle and matter [4]. In our simulation, the primary proton beam is up to 250MeV, gamma and neutron are secondary particles that contribute most to the radiation effect. We employ GQSP_BIC_HP to be the reference physics list in the simulation.

To build a balance between physics precision and CUP performance, the range cut used in the simulation is default 0.7mm and each run consists of 2×10^6 primary events. The proton beam irradiates the center of normal septum surface along the +Z axis, inducing p-W, p-Ta or p-Mo nuclear interactions.

As shown in Fig. 1, the incident proton beam (blue) impinges the septum producing secondary particles, most of which are gammas (red) and neutrons (green).

RESULTS AND DISCUSSION

Energy Depositions on the Septum

SRIM software calculates the Bragg peak depth and maximum energy deposition of above three materials. The results are listed in Table 2.Then we use Geant4 to do the same work and plot the energy deposition curves as a function of depth in Fig. 2. Note that the macro-file based scoring commands are adopted to record the energy deposition in Geant4, when the 250MeV proton beam irradiates the large enough material bulks (100mm×100mm×200mm) so that its energy is postulated to be fully deposited in the bulks. It's pleased to see that the results from Geant4 agrees well with the data obtained with SRIM with regard to Bragg peak and maximum energy deposition.

Table 2: A List of Calculated Results from SRIM

Material	Atom number (Z)	Bragg peak depth (mm)	Maximum energy deposition (MeV/mm)
W	74	37.51	1.44
Ta	73	43.66	1.25
Mo	42	59.75	0.97

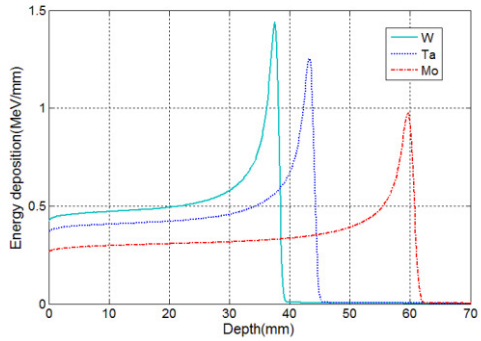

Figure 2: Energy deposition curves of 250MeV proton beam in three materials.

Obviously seen from Table 2 and Fig. 2, we know that the tungsten exhibits the shortest Bragg peak depth and highest maximum energy deposition. However, in practical operating conditions, the septum is so thin, only 0.3mm, that the energy of proton beam won't be completely deposited. Since the positon where the maximum energy deposition locates indicates the fiercest heating effect and nuclear interactions, it is essential to illustrate the distribution of energy deposition on the septum shown in Fig. 3.

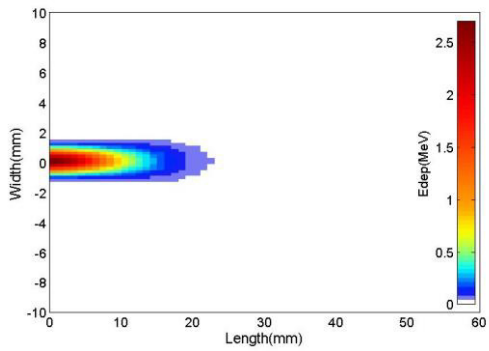

Figure 3: Distribution of energy deposition on the tungsten septum.

As displayed in Fig 3, the energy deposition mostly occurs on the leading edge of the septum. The dimension of the main energy deposition area reaches nearly 20mm×3mm where the fiercest nuclear interactions happens.

Yields and Energy Distributions of Secondary Particles

The ratio between the number of generated secondary particles and primary proton number presents the normalized yields of secondary particles. The metal blocks (100mm × 100mm × 200mm) are irradiated by 250MeV proton beam to observe various radiation characteristics of three materials. The yields in the case of beam hitting 0.3mm thin septum are computed as well. The yields of secondary neutron and gamma are given in Table 3.

Table 3 demonstrates that high Z material produces more secondary particles. Compare the yields in block and septum, the yields of neutron are almost the same while the yields of gamma show a large variance. The yield of

ISBN: 978-3-95450-184-7 doi:10.18429/JACoW-IPAC2018-TUPAK013

gamma in block is apparently higher than that in septum. An explanation for this discrepancy is that the generation of secondary gamma requires more interaction time than neutron, thus hadron shower for gamma has not been fully developed in the septum.

Table 3:Yields of Gammas and Neutrons

Material (Z)	Yield in block		Yield in septum	
	neutron	gamma	neutron	gamma
W (74)	3.694	5.608	3.692	1.483
Ta (73)	3.571	5.428	3.522	1.407
Mo (42)	1.601	2.427	1.574	1.250

The energy distributions of secondary gamma and neutron in the above two cases are shown in Fig. 4 and Fig. 5.

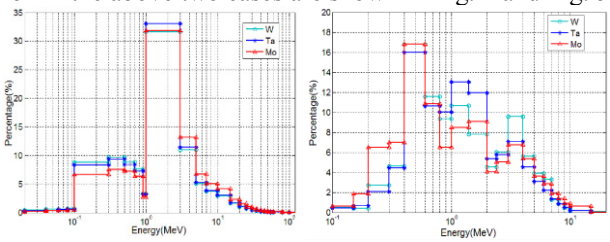

(a) (b)

Figure 4: Energy distributions in block. (a): secondary neutron; (b): secondary gamma.

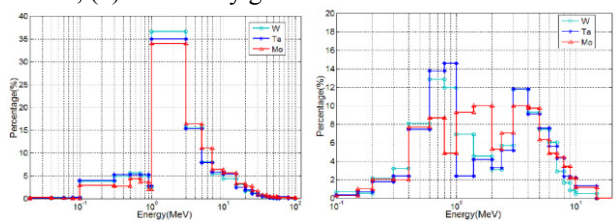

(a) (b)

Figure 5: Energy distributions in septum. (a) : secondary neutron; (b): secondary gamma.

As shown in above graphs, no matter in the case of block or septum, the energy distributions of secondary neutron are almost the same. More than 90% of the neutron gathers in 0-15MeV energy range and the energy of more than half of generated neutrons lies below 3MeV. Moreover, tungsten tends to produce neutron below 1MeV and molybdenum is inclined to generate neutron above 3MeV inferring from the percentage of corresponding neutron energy among three materials.

The energy distributions of gamma differ from that of neutron. The energy of secondary gamma relatively low mainly ranging from 0-4MeV accounting for more than 80% of total. In the case of block, molybdenum produces more gamma below 1MeV than tantalum and tungsten. However things are opposite in the case of septum.

Those results may bring some implications for the radiation shielding designers.

Angular Distributions of Secondary Particles Flux

The generated secondary particles project to diverse directions because of the collision between septum and beam. Based on the preceding discussions, tungsten is more likely to produce secondary particles than tantalum and molybdenum. Therefore we choose tungsten as the simulation material to record angular distribution of secondary particles for a conservative consideration. Two cases are set up for the research: one is the proton beam shoots normally to the entrance face, the other is slant proton beam set for 10° inward angel to impinge the septum lateral surface. The angular distributions of secondary neutron and gamma are displayed in Fig. 6.

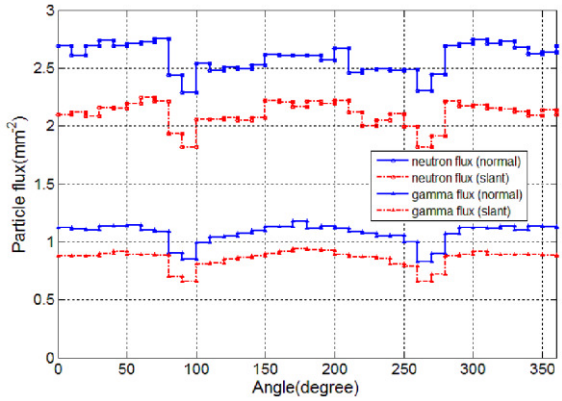

Figure 6: Angular distribution of secondary particle flux.

Figure 6 tells that the secondary particle flux in slant shoot case is comparatively smaller than that in normal shoot case. This probably results from the short interaction time when the slant beam rapidly penetrates through the thin septum. The stair curves in the figure is symmetrical to some extent. For neutron and gamma, the minimum flux appears in the 90° -100° and 260° -270° zone, while the flux is slightly higher in the housing direction(150° -200° zone). Designers should pay attention to the flux distributions when they consider radiation protection.

CONCLUSION

Using Geant4 code, this paper exhibits a detailed study into radiation effect caused by beam impinging on the septum. The energy depositions on the septum demonstrate that the leading edge of deflector is confronted with strongest nuclear interaction and highlight the need for dealing with radiation effect. Tungsten seems to produce fiercest radiation effect among the simulated materials since the yields of secondary particles are highest. The energy and angular distributions of secondary particles provide useful implications for researchers to shield neutron and gamma in specific energy ranges and angle zones. In the future work, we will improve the simulation model and method for a more detailed investigation. The simulation data should/will be benchmarked with measurements.

ACKNOWLEDGEMENT

This work was supported by the Science Foundation of the Chinese Academy of Sciences under Grant 11775087, the National Program for Research and Development of Digital Diagnostic Equipment Project under Grant 2016YFC0105303 and the Chinese Academy of Sciences under Grant 11505068.

ISBN: 978-3-95450-184-7 doi:10.18429/JACoW-IPAC2018-TUPAK013

REFERENCES

[1] S. Hu *et al.,* "Design and fluid-solid-heat coupling analysis of an electrostatic deflector for HUST SCC250 proton therapy facility", in *Proc. IPAC'17*, Copenhagen, Denmark, May 2017, paper THPVA109, pp. 4713-4715.

[2] Z. S. Hartwig *et al*., "Nuclear heating and radiation damage studies for a compact superconducting proton cyclotron", submitted for publication.

[3] S. Incerti *et al.,* "Simulation of cellular irradiation with the CENBG microbeam line using Geant4", submitted for publication.

[4] J. Apostolakis *et al.,* "GEANT4 physics lists for HEP", submitted for publication.